Role of ethylamines on the electrochemical behaviour of Fe–Ni alloy films

C.L. ARAVINDA[1], V.S. MURALIDHARAN[2] and S.M. MAYANNA[1]*
[1]*Department of Post-graduate Studies in Chemistry, Central College, Bangalore University, Bangalore 560 001, India*
[2]*Central Electrochemical Research Institute, Karaikudi 630 006, India*
(*author for correspondence)*

Abstract

Cyclic voltammetric experiments were carried out on platinum in acidic solution (pH 3) containing ferrous sulfate, nickel sulfate and ethylamines ($EtNH_2$, Et_2NH, Et_3N). Spectral ultraviolet absorption studies indicate the complexation of both Fe^{2+} and Ni^{2+} ions with ethylamines. The results under transient polarisation conditions indicate the reduction of Fe^{2+} ions through the intermediate species $FeOH^+$, with second electron transfer as a slow step. The higher charge transfer rate of $FeOH^+$ over $NiOH^+$ reduction causes the anomalous codeposition of Fe–Ni alloy film. Among the ethylamines, Et_3N considerably assists the alloy deposition process. A gradual variation in free energy of alloy formation with $Fe^{2+}:Ni^{2+}$ (mol:mol) in the bath suggests the formation of an alloy intermediate phase rich in iron. Stripping voltammetric curves indicate the preferential dissolution of iron from iron rich alloy intermediate phase. X-ray diffraction studies further confirm the phase to be b.c.c. Fe–Ni alloy. The extent of corrosion of the Fe–Ni alloy film in the presence of ethylamines is in the following order: Et_3N > Et_2NH > $EtNH_2$.

1. Introduction

Electrodeposited thin films of Fe–Ni alloys are extensively used in the microelectronic industries for a variety of applications [1, 2]. The recent emergence of microstructuring and microsystem fabrication by the LIGA process [3, 4] illustrates the potential candidature of Fe–Ni alloy films for newer applications such as fabrication of microacutuators and solenoids [5–7]. The corrosion and magnetic properties of the electrodeposited Ni–Fe permalloys depend greatly on their crystallinity, grain size, thickness, bath composition and additives used. Reviews on the subject are noteworthy [8, 9].

Numerous Fe–Ni alloy plating baths have been developed in the last two decades [10, 11]. However, amines are often used in the plating bath solutions since their presence greatly affects the phenomenon of anomalous codeposition [12]. Attempts have been made to produce Ni–Fe alloy films of varying composition and magnetic properties from acidic bath solutions containing various alkyl amines [13]. Most of the earlier work has been directed towards the understanding of the anomalous codeposition phenomenon. Despite having both practical and theoretical importance, the role of ethylamines on the electrochemical behaviour of Fe–Ni alloy films is not well understood. The present communication describes a cyclic voltammetric study of the role of ethylamines on the electrochemical behaviour of Fe–Ni alloy deposits on platinum in acidic solution.

2. Experimental details

All solutions were prepared using double distilled water and AR grade chemicals. Predistilled ethylamines: monoethylamine ($EtNH_2$), diethylamine (Et_2NH) and triethylamine (Et_3N) of known concentration (0.05 M < x < 0.15 M) were used along with $FeSO_4 \cdot 6H_2O$ (0.01 M < x < 0.1 M), $NiSO_4 \cdot 6H_2O$ (0.01 M < x < 0.1 M), boric acid (0.05 M) and sodium chloride (10 g L^{-1}). The pH of the medium was maintained at 3 by adding dilute sulfuric acid using a digital pH meter.

Experiments were carried out in an all glass single compartment cell of 50 ml capacity at 298 K. A miniature platinum wire was used as a working electrode along with a large platinum foil and saturated calomel electrode as auxiliary and reference electrodes, respectively. A finely drawn luggin capillary was used to minimize the IR drop. The platinum electrodes were precleaned by a standard procedure [14]. N_2 gas was bubbled continuously through the solutions to limit the oxidation of Fe^{2+} ions by oxygen. Cyclic voltammograms were obtained at various sweep rates (10–100 mV s^{-1}) by monitoring the desired potential using

a potentiostat (EG&G PAR 362) and only reproducible responses were recorded. Ultraviolet absorption studies were made using a spectrometer (Hitachi 150-20, Japan). An X-ray diffractometer (Siemen D5005) with CuK_α radiation was used to characterise the phases of the deposited alloy films.

3. Results

3.1. Cyclic voltammetric studies

Figure 1 shows the cyclic voltammograms obtained in the solution containing Et_3N and Fe^{2+} ions. The forward scan exhibits two cathodic peaks at -654 mV ($1c_1$) and -954 mV ($1c_2$), respectively. During the reverse scan a hump appears at -652 mV followed by a sharp peak ($1a_1$) at -544 mV. On repeated cycling between 0 and -1100 mV, the cathodic peak ($1c_1$) shifts to more negative potentials while, the peaks ($1c_2$) and ($1a_1$) remain unaltered. However, the charge under the peak decreases. The peak potential ($1c_1$) varies linearly with sweep rate (v) resulting in a slope of 40 mV dec^{-1} and the peak potential difference, that is, $\Delta E_p[E_{p,c}(1c_1) - E_{p,a}(1a_1)]$ varies linearly with log[amine] with a slope of 100 mV dec^{-1}.

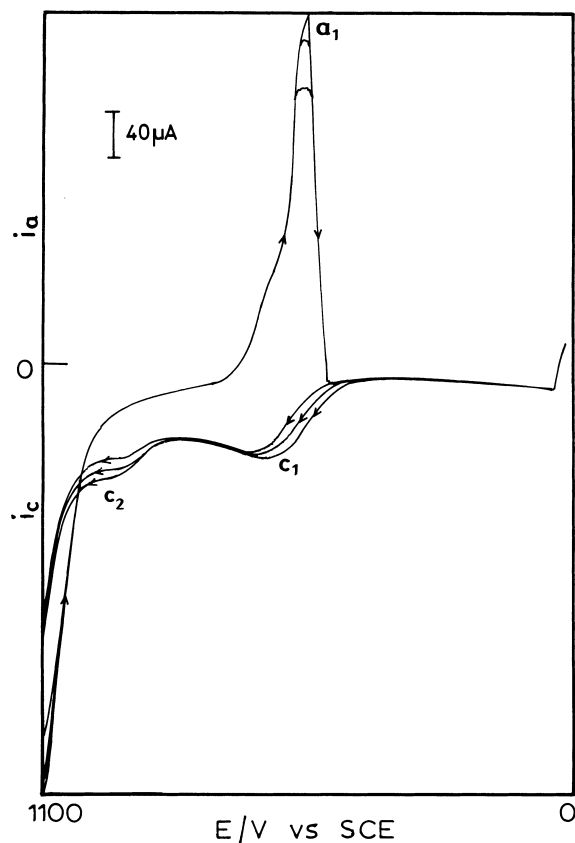Figure 2 shows the voltammograms obtained in solution containing Ni^{2+} ions and Et_3N. The forward
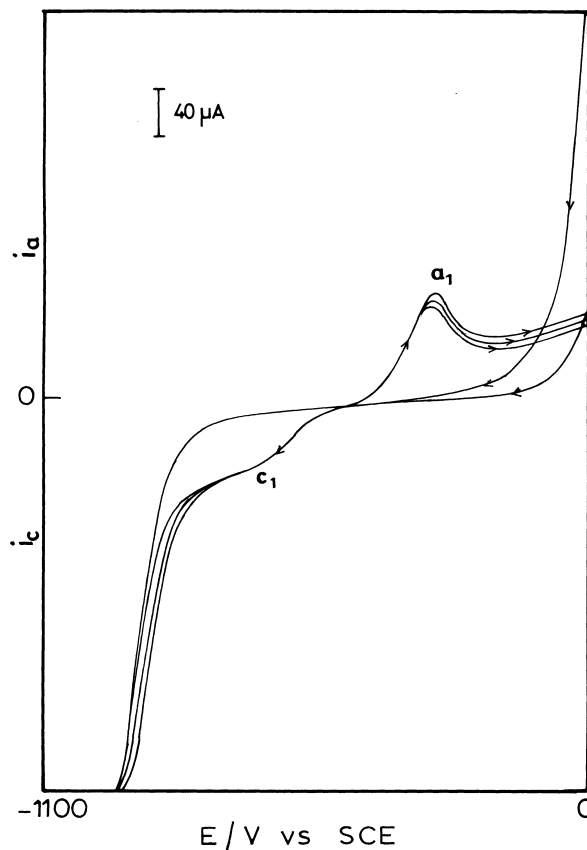

Fig. 2. Effect of cycling on cyclic voltammograms obtained in solution containing $NiSO_4$ 0.15 M, Et_3N 0.02 M, NaCl 10 g L^{-1}, H_3BO_3 0.05 M at pH 3 and $v = 10$ mV s^{-1}.

scan exhibits a cathodic peak ($2c_1$) at -710 mV followed by a sharp rise in current beyond -900 mV. On repeated cycling, the peak potential becomes more negative with a decrease in charge under the peak. During the reverse scan a single anodic peak ($2a_1$) appears at -314 mV. The peak potential difference $\Delta E_p[E_{p,c}(2c_1) - E_{p,a}(2a_1)]$ varies linearly with log [amine] with a slope of 40 mV dec^{-1}.

Figure 3 shows the cyclic voltammograms obtained in the solution of Et_3N containing various molar ratios of $Fe^{2+}:Ni^{2+}$. In the 1:0.25 molar solution, the forward scan exhibits a plateau ($3c_1$) around -602 mV, which becomes a peak ($3c_2$) at -672 mV with decrease in nickel content (1:05). During the reverse scan the zero current crossing potential (ZCCP) occurs at -600 mV followed by an anodic peak ($3a_1$) at -506 mV. When the molar concentration ratio of metal ions is changed to 1:1, the forward scan gives a peak ($3c_4$) at -678 mV followed by a sharp anodic peak ($3a_4$) at -406 mV during the reverse scan. The anodic peak potential becomes more positive with increase in Ni^{2+} ion concentration. A similar trend in the behaviour of iron and nickel was also observed in the presence of Et_2NH and $EtNH_2$.

3.2. Chronoamperometric transients

Figure 4 shows chronoamperometric responses for the nucleation and growth of Fe–Ni alloy on a platinum
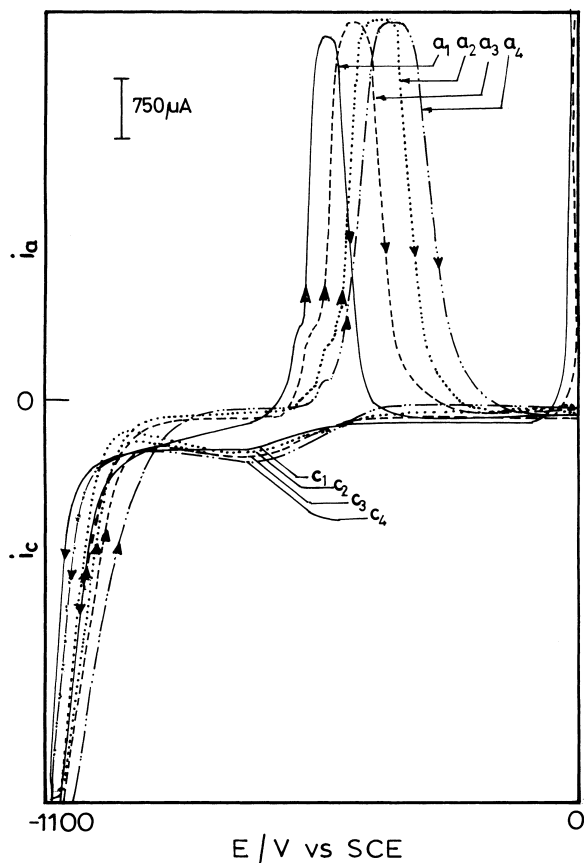

Fig. 1. Effect of cycling on cyclic voltammograms obtained in solution containing $FeSO_4$ 0.15 M, Et_3N 0.02 M, NaCl 10 g L^{-1}, H_3BO_3 0.05 M at pH 3 and $v = 10$ mV s^{-1}.

Fig. 3. Cyclic voltammograms obtained in solutions of varying Fe:Ni/mol:mol (keeping $[Fe^{2+}]$ = 0.15 M with Et_3N 0.02 M, NaCl 10 g L^{-1}, H_3BO_3 0.05 M at pH 3 and v = 10 mV s^{-1}): (1) 1:0.25, (2) 1:0.5, (3) 1:0.75 and (4) 1:1.

electrode kept at −0.9 V in solution with and without ethylamines. An initial decay in current followed by a gradual increase is observed. Initially, there is a possibility that most of the surface is covered by Fe–Ni alloy, while H_2 evolution (HER) occurs on exposed platinum. After an initial delay of 0.2 s and beyond 1 s the platinum surface is covered entirely by alloy film. The erratic responses observed are due to HER, which occurs only on the continuously deposited alloy film. The calculation of charge during cyclic voltammetry in the potential range 0 to −1100 mV indicates the formation of more than one monolayer. It follows that there is a competition between H_2 evolution and deposition of new phase onto the platinum surface as it offers lower H_2 overvoltage. Increase in the growth current with respect to alloy deposition shows that the presence of ethylamines in the bath favours the alloy deposition process, the extent of which is higher with Et_3N.

3.3. *UV absorption spectral studies*

The electronic absorption spectrum (Figure 5) of an aqueous solution of Fe^{2+} ions containing Et_3N shows an intense metal–ligand charge transfer split band around 390 nm, which is associated with the six coordinated complex of Fe^{2+} ions with Et_3N leading to a complex with a structure $[Fe(H_2O)_4L_2]^{2+}$, where L is the ethylamine. A similar spectral study with an aqueous solution containing Ni^{2+} ions and Et_3N shows peaks at 390 nm, 648 nm and 728 nm. Based on these data, the assigned [15] transitions are $^3T_1g(P) \leftarrow {}^3A_2g$ (v_3), $^3T_1g \leftarrow {}^3A_2g$ (v_2) and $^3T_2g \leftarrow {}^3A_2g$ (v_1), respectively, for Ni^{2+} ion in an octahedral arrangement leading to a complex with a structure $[NiL_6]^{2+}$. Similar results were obtained regarding the complexation of Fe^{2+} ions ad Ni^{2+} ions with Et_2NH and $EtNH_2$.
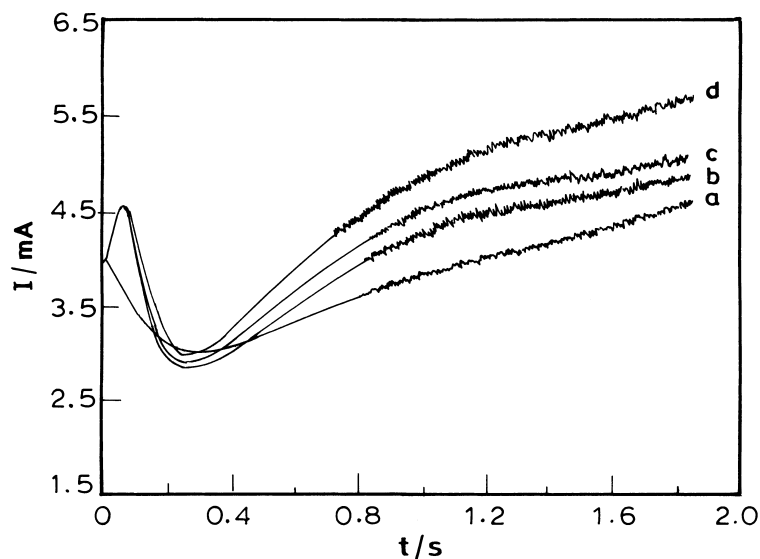

Fig. 4. Influence of amines on chronoamperometric responses (solution composition: $FeSO_4$ 0.15 M, $NiSO_4$ 0.15 M, [amine] = 0.15 M, NaCl 10 g L^{-1}, H_3BO_3 0.05 M, pH 3 at a potential step of 0.9 V: (a) without (b) $EtNH_2$, (c) Et_2NH and (d) Et_3N.
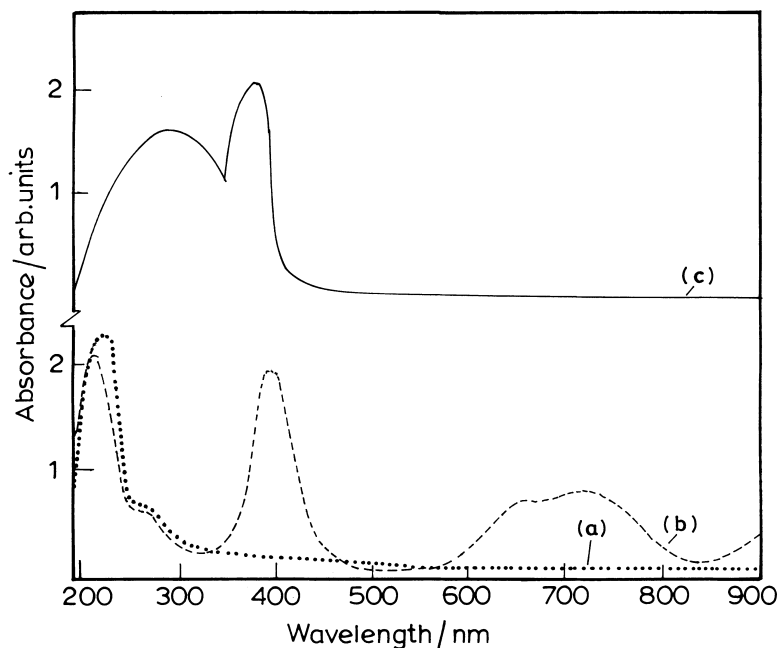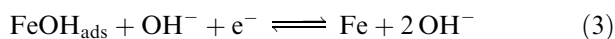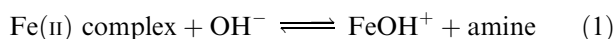
Fig. 5. UV absorption spectra of solutions/0.1 M: (a) Et_3N, (b) $NiSO_4$ and (c) $FeSO_4$.
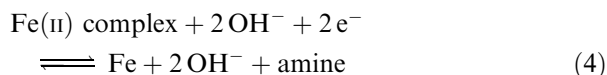
4. Discussion

4.1. *Electrochemical behaviour of iron and nickel*

The appearance of the cathodic peak (Figure ($1c_1$)) is due to the reduction of Fe(II) complex to iron followed by H_2 evolution from the protonated amine at pH 3. The deposition of iron may occur from Fe(II) complex through consecutive steps.

$$Fe(II) \text{ complex} + OH^- \rightleftharpoons FeOH^+ + amine \quad (1)$$

$$FeOH^+ + e^- \rightleftharpoons FeOH_{ads} \quad (2)$$

$$FeOH_{ads} + OH^- + e^- \rightleftharpoons Fe + 2OH^- \quad (3)$$

The overall reaction is

$$Fe(II) \text{ complex} + 2OH^- + 2e^-$$
$$\rightleftharpoons Fe + 2OH^- + amine \quad (4)$$

If the discharge (step 2) is slow and irreversible [16] then we can write

$$E_{p,c} = E^\circ - \left(\frac{RT}{\alpha_c F}\right)\left[\ln\left(\frac{D_0}{k_0}\right)^{0.5} + \ln\left(\frac{\alpha_c F v}{RT}\right)^{0.5} + 0.78\right]$$
$$(I)$$

where $E_{p,c}$ is the cathodic peak potential, v is the sweep rate, D_0 and α_c are the diffusion coefficient and transfer coefficient of the Fe(II) complex, respectively. The plot of $E_{p,c}$ against log v would give $-\alpha_c F/RT$ and a slow second electron transfer reaction could give a value of 40 mV dec^{-1}. This is in agreement with the observed value of cathodic Tafel slope, which suggests that the Fe(II) complex undergoes successive reduction in which the second electron transfer is slow.

The Nernst equation for the overall reaction (Equation 4) takes the form

$$E_{r,Fe} = E_{Fe}^\circ + 2.303\left(\frac{RT}{2F}\right)\log\left(\frac{[Fe][amine]}{Fe(II) \text{ complex}}\right) \quad (II)$$

where E_{Fe}° is the standard potential of iron.

It can be shown that

$$\Delta E_p = 2.303\left(\frac{RT}{2F}\right)\log\left(\frac{[Fe][amine]}{Fe(II)complex}\right) \quad (III)$$

The dependence of ΔE_p with log [amine] with a slope of 100 mV dec^{-1} suggests that amines have not complexed completely with Fe^{2+} ions. Amines in the protonated form may undergo reduction to liberate hydrogen.

The electrochemical behaviour of nickel can be explained in a manner similar to that for iron. The observed cathodic peak at -710 mV is due to the reduction of Ni^{2+} complex and the sharp rise in cathodic current beyond -900 mV is due to hydrogen evolution on freshly deposited nickel film. It was shown earlier that deposition and dissolution of nickel in acidic solutions involves the formation of $NiOH^+$ intermediate species [17]. The observed cathodic Tafel slope 40 mV dec^{-1} suggests that the Ni(II) complex undergoes successive reduction and the second electron transfer is slow, as in the case of iron with the overall reaction:

$$Ni(II) \text{ complex} + 2OH^- + 2e^-$$
$$\rightleftharpoons Ni + 2OH^- + amine$$
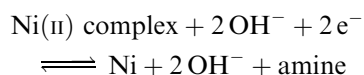
4.2. Electrochemical behaviour of Fe–Ni alloy film

Many deposition models have been proposed [18, 19] to explain the phenomenon of anomalous codeposition of Fe–Ni alloy [8]. Usually the deposition of Ni–Fe alloy proceeds with a simultaneous discharge of Ni^{2+} and Fe^{2+} ions under activation control along with hydronium ions under mass transfer control. In the present study, the observed cathodic peak at -672 mV followed by hydrogen evolution suggests that the charge transfer rate of $FeOH^+$ is faster than $NiOH^+$ reduction which occurs along with the hydrogen evolution. As a result of the competition between $NiOH^+_{ads}$ and $FeOH^+_{ads}$ for the available active sites, the preferential deposition of iron occurs over nickel.

4.3. Intermediate phase formation

During Fe–Ni alloy deposition the formation of an alloy intermediate or intermetallic phase can be visualized from the reversible potential of Fe/Fe^{2+} ions in the solution, which is given by

$$E_{r,Fe} = E^\circ_{Fe} + \left(\frac{RT}{2F}\right) \ln\left(a_{Fe(II) \text{ complex}}\right) \quad \text{(IV)}$$

where E°_{Fe} is the standard potential for iron

$$E_{r,Fe\text{-alloy}} = E^\circ_{Fe} + \left(\frac{RT}{2F}\right) \ln\left(\frac{a_{Fe(II) \text{ complex}}}{a_{Fe\text{-alloy}}}\right) \quad \text{(V)}$$

$E_{r,alloy}$ is the reversible potential of iron in the alloy intermediate phase (it is assumed that the surface energy contribution at the alloy–electrolyte interface is negligible).

The difference (Equation IV − Equation V) is thus:

$$-\Delta E = E_{r,Fe} - E_{r,Fe\text{-alloy}} = \left(\frac{RT}{2F}\right) \ln\left(a_{Fe\text{-alloy}}\right) \quad \text{(VI)}$$

$$2F\Delta E = RT \ln\left(a_{Fe\text{-alloy}}\right) = -\Delta G \quad \text{(VII)}$$

From the difference in the anodic peak intersection potentials both for iron and Fe–Ni alloy intermediate phase, the free energy of alloy formation can be calculated [20]. Figure 6 gives the variation of ΔG with different Ni^{2+}/Fe^{2+} (mol/mol) composition in various amine solutions, which suggests the formation of an alloy intermediate phase [21]. This is further confirmed by the XRD studies (Figure 7) on the film deposited from the 1:1 (Fe^{2+}:Ni^{2+}) molar solution, which shows a mixture of f.c.c. and b.c.c. phases. However, the alloy obtained from a bath containing Fe^{2+} and Ni^{2+} ions in the molar ratio 1:0.25 shows only b.c.c. phase. Recently, Osaka and coworkers showed that additives determine phase boundaries of f.c.c. and b.c.c. phases [22]. Such phase separation into f.c.c. and b.c.c. is more pronounced in the case of electrodeposited nanocrystalline alloys when compared to thermally alloyed metals [23].

4.4. Corrosion behaviour

The value of ZCCP in a solution is an indication of the susceptibility of the alloy film to corrosion. Introduction of Ni^{2+} and increase in Ni^{2+}/Fe^{2+} (mol/mol) composition shifts the ZCCP values in the noble direction. Under similar experimental conditions, the obtained ZCCP values (Figure 8) in the presence of ethylamines suggest that the solution containing Et_3N is most corrosive. The dissolution currents obtained from the foot of the anodic peaks in the presence of ethylamines are in the order: $i_{Et_3N} > i_{Et_2NH} > i_{EtNH_2}$. Figure 9 represents $E/\log I$ curves for alloy dissolution in Et_3N
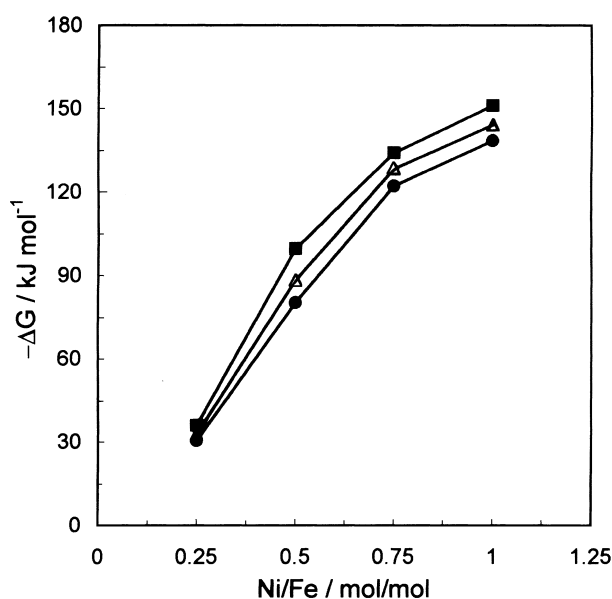

Fig. 6. Variation of ΔG in solutions of different amines with varying Ni^{2+}/Fe^{2+} molar concentration (keeping $[Fe^{2+}] = 0.15$ M, NaCl 10 g L^{-1}, H_3BO_3 0.05 M at pH 3). Key: (●) $EtNH_2$, (△) Et_2NH, (■) Et_3N.

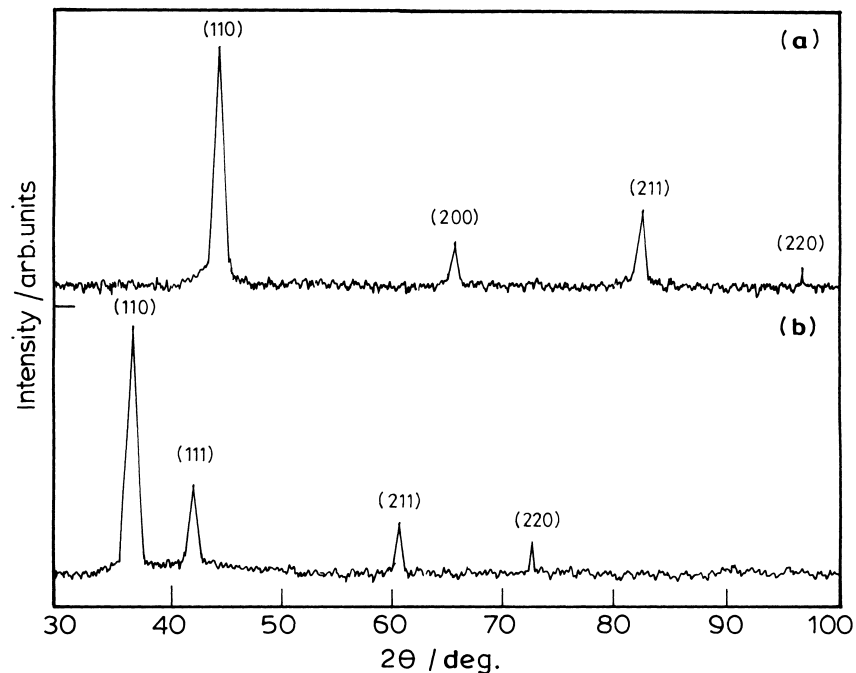*Fig. 7.* XRD patterns obtained on Fe–Ni alloy films deposited at -1100 mV from solutions containing varying $Fe^{2+}:Ni^{2+}$/mol:mol composition (keeping $[Fe^{2+}] = 0.15$ M, $Et_3N = 0.15$ M, NaCl 10 g L^{-1}, H_3BO_3 0.05 M, at pH 3): (a) 1:1, (b) 1.025.
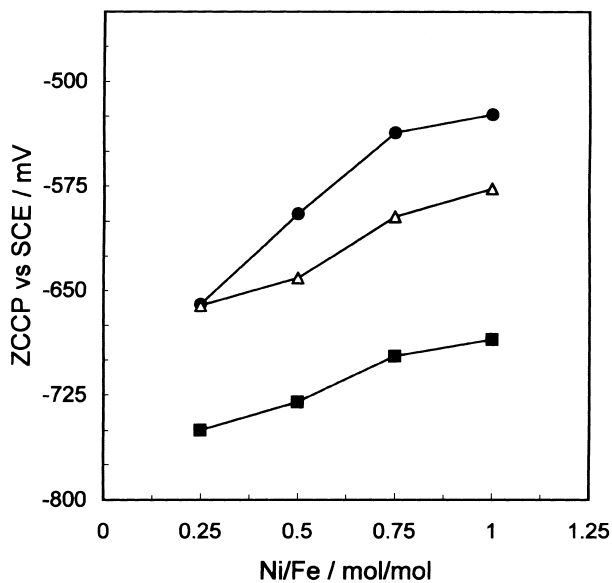

Fig. 8. Variation of zero current crossing potential (ZCCP) in solutions of different amines with varying Ni^{2+}/Fe^{2+} molar concentration (keeping $[Fe^{2+}] = 0.15$ M, NaCl 10 g L^{-1}, H_3BO_3 0.05 M, at pH 3). Key: (●) $EtNH_2$, (△) Et_2NH, (■) Et_3N.

Fig. 9. *E* against log *I* curves for iron dissolution in the solutions of varying $Fe^{2+}:Ni^{2+}$/mol:mol composition (keeping $[Fe^{2+}] = 0.15$ M, NaCl 10 g L^{-1}, H_3BO_3 0.05 M, at pH 3). Key: (●) 1:0, (△) 1:0.5, (■) 1:1.

Table 1. Parameters obtained from *E* against log *I* curves

Solution composition $Fe^{2+}:Ni^{2+}$ /mol:mol	Zero current crossing potential /mV	$I_{corr}/\mu A$	Anodic Tafel slope /mV dec^{-1}	Phases obtained*
1:0.25	-715	8.9	40	b.c.c.
1:0.5	-590	3.18	120	–
1:1	-565	3.16	120	f.c.c. + b.c.c.

* *Figure 7.*

solution containing various molar compositions of Fe^{2+} and Ni^{2+} ions. The corrosion current obtained by the extrapolation of the linear segment of the curve to ZCCP is found to be less for the film obtained from 1:1 ($Fe^{2+}:Ni^{2+}$) molar solution (Table 1). The change in anodic Tafel slope for iron dissolution from the alloy suggests that the presence of nickel alters the dissolution mechanism. The preferential dissolution of iron occurs
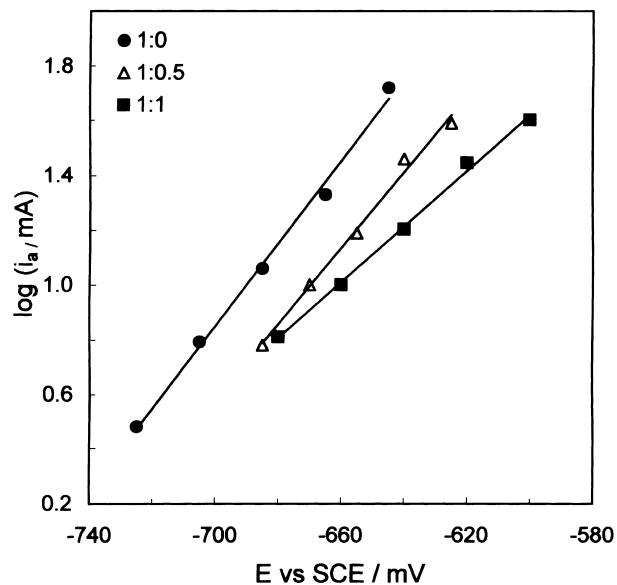
from Fe–Ni alloy intermediate phase rich in iron, notably from the b.c.c. alloy phase rather than f.c.c. alloy phase which offers better corrosion resistance [24].

5. Conclusions

The higher charge transfer rate of $FeOH^+$ over $NiOH^+$ reduction causes the anomalous codeposition of Fe–Ni alloy film. The ethylamines especially, Et_3N which forms a complex with both Fe^{2+} and Ni^{2+} ions, favours the alloy deposition process. Deposited alloy films assist the HER from solution containing ethylamines. The gradual variation in free energy with increase in nickel content during alloy deposition indicates the existence of alloy intermediate phase. The presence of nickel in the deposit modifies the dissolution mechanism, which involves the preferential dissolution of iron from alloy intermediate phase rich in iron. XRD studies confirm the phase to be b.c.c. Fe–Ni alloy. Et_3N solution is more corrosive than Et_2NH or $EtNH_2$ solution for Fe–Ni alloy film.

Acknowledgement

References

1. C.A. Ross, *Ann. Rev. Mater. Sci.* **24** (1994) 159.
2. B. Lochel, A. Maciossek, H.J. Quenzer and B. Wagner, *J. Electrochem. Soc.* **143** (1996) 237.
3. A. Thommes, W. Stark, K. Leyendecker, W. Bacher, H. Leibscher and Ch. Jakob, 'LIGA Microstructures From a Ni–Fe Alloy: Preparation by Electroforming and their Magnetic Properties', *Electrochem. Soc. Proc.* **94–6** (1994) 89–102.
4. B. Lochel and A. Maciossek, *J. Electrochem. Soc.* **143** (1996) 3343.
5. D. Sadler, W. Zhang, C.H. Ahn, H.J. Kim and S.H. Han, *IEEE Trans. Mag.* **33** (1997) 3319.
6. T.M. Liakopoulos, M. Xu and C.H. Ahn, *in* 'Technical Digest: 1998 Solid-State Sensor and Actuator Workshop' (Transducers Research Foundation, Hilton Head, SC, 1998), pp. 19–22.
7. T. Lorenz, M. Moske, H. Kufler, H. Geisler and K. Samwer, *J. Appl. Phys.* **78** (1996) 4765.
8. T. Akiyama and H. Fukushima, *ISIJ Intl.* **32** (1990) 787.
9. S.S. Djokic and M.D. Maksimovic, *in* J.O'M Bockris, R.E. White and B.E. Conway (Eds), 'Modern Aspects of Electrochemistry', Vol. 22 (Plenum Press, New York, 1992), pp. 417–466.
10. S.N. Srimathi, S.M. Mayanna and B.S. Sheshadri, *Surf. Technol.* **6** (1982) 277.
11. P.C. Andricacos and L.T. Romankiw, *in* H. Gerischer and C.W. Tobias (Eds), 'Advances in Electrochemical Science and Engineering', Vol. 3 (VCH, Weinheim, 1994), pp. 227–321.
12. T.M. Harris and J.L. St. Clair Wilson, *in* M. Paunovic and D.A. Scherson (Eds), 'Electrochemically Deposited Thin Films III', PV 96–19, (The Electrochemical Society Proceedings Series, Pennington, NJ, 1996), p. 227.
13. S.N. Srimathi and S.M. Mayanna, *J. Appl. Electrochem.* **13** (1983) 679.
14. R. Greef, R. Peat, L.M. Peter, D. Pletcher and J. Robinson, 'Instrumental Methods in Electrochemistry' (Ellis Horwood, Chichester, 1985), p. 359.
15. A.B.P. Lever, 'Inorganic Electronic Spectroscopy' (Elsevier Publishing Company, London, 1968), pp. 299–349.
16. D.D. Macdonald, 'Transient Techniques in Electrochemistry' (Plenum Press, New York, 1977), p. 193.
17. V.S. Muralidharan, M. Veerashunmugamani, G. P. Kalaignan and S. Arulraj, *Bull. Electrochem.* **1** (1985) 241.
18. M. Motlosz, *J. Electrochem. Soc.* **140** (1993) 2272.
19. C. Baker and A.C. West, *J. Electrochem. Soc.* **144** (1997) 169.
20. A.R. Despic and V.D. Jovic, *in* J.O'M Bockris, R.E. White and B.E. Conway (Eds), 'Modern Aspects of Electrochemistry', Vol. 27 (Plenum Press, New York, 1995), p. 225.
21. D.A. Porter and Y.A. Easterling, 'Phase Transformations in Metals and Alloys' (Workingham, Van NonStrand Reinhold, 1980).
22. T. Osaka, M. Takai, Y. Sagawa, T. Momma, K. Ohashi, M. Saito and K. Yamada, *J. Electrochem. Soc.* **146** (1999) 2092.
23. K.S. Werkmeister, M. Heyer, M. Coach, F. Rullang and G. Schwitzgeble, *Nanosturct. Mater.* **12** (1999) 229.
24. I. Tabakovic, S. Riemer, V. Inturi, P. Jallen and A. Thayer, *J. Electrochem. Soc.* **146** (2000) 219.